**Guiting Xue[1], Yan Zhang[1], Dakang Zhu[2]**

Shanghai Jiaotong University (1), Shanghai Municipal Electric Power Company (2)

# Optimal Power Assignment and Coordinated Control Strategy for a Small-Scale Residential DC Microgrid

***Abstract***. *This paper focuses on control and operation of a small-scale residential dc microgrid supplied by photovoltaic array (PVA), fuel cell (FC) and super-capacitor (SC). The control scheme aims to realize the optimal power allocation, protect FC from fuel starvation, and stabilize dc bus voltage. The dc microgrid can operate in both islanded and grid-connected mode. To make the system work properly during islanding operation, power control and energy management strategy are proposed. When system is grid-connected, power balance is achieved by controlling the three-phase voltage source rectifier (VSR). The effectiveness of the proposed control method is verified through simulations.*

***Streszczenie.*** *W artykule skupiono się na zagadnieniu sterowania mikro-siecią DC małej skali w zastosowaniu mieszkaniowym, zasilanej z systemu złożonego z paneli fotowoltaicznych (ang. photovoltaic array), ogniw paliwowych (ang. fuel cell) oraz super-kondensatora (ang. super-capacitor), z naciskiem na optymalizację rozpływu mocy, zapewnienie dopływu paliwa dla ogniw paliwowych i stabilizację napięcia DC. Przeprowadzono analizę symulacyjną algorytmu, gdzie rozważono przypadki pracy wyspowej i podłączenia do sieci energetycznej. (**Kompleksowe sterowanie i optymalizacja rozpływu mocy w mikro-sieci DC małej skali w zastosowaniu mieszkaniowym**).*

**Keywords:** dc microgrid, distributed generation, coordination control, Islanding
**Słowa kluczowe:** micro-sieć DC, generacja rozproszona, sterowanie kompleksowe, praca wyspowa.

## 1. Introduction

In recent years, more and more distributed generations (DGs) are being installed into power system. But if a large number of DGs are installed into utility grid, they will cause problems such as voltage rise and protection issue. As a solution for smooth installation of DGs, microgrid was introduced [1]. At present, most of the microgrids adopt ac distribution, and most of the literature studied so far have concentrated on ac microgrids, which have several disadvantages including synchronization requirements for multiple microsources, reactive power flow, and circulating currents due to differences in voltage magnitude, phase angle, or dc offset in a multi-inverter system [2].

Compared with ac microgrid, dc microgrid can enable easier interconnection of renewable energy sources. Because many of them, such as photovoltaic array (PVA), fuel cell (FC) and super-capacitor (SC) are natively dc sources. Adopting dc microgrid can reduce the number of conversion stages, thereby decreasing the system losses [3]. On the other hand, dc loads (e.g., electric vehicle and electronic devices, etc.) can be directly supplied by low voltage dc power system. Furthermore, power electronic interfaces for DGs have the ability to control the voltage and current disturbances. As a result, dc microgrids have now received a considerable attention from scholars and electric utility industry.

DC distribution systems at lower voltage levels are mainly used in commercial buildings [4, 5], and residential applications [3, 6] where sensitive loads benefit from increased power quality and reliability [7] which results in cost savings and increase in electrical conversion efficiency [5]. Coordinated control strategy for dc distribution networks under different operation modes has been studied [8, 9]. However, load shedding is inevitable in the aforesaid system because energy storage devices have limited capacity. Moreover, load shedding also is a more complex thing [9]. In [10], the dc distribution system including microturbine, fuel cell units, and battery storage bank has been studied. But the method to avoid fuel starvation is not described in detail.

From the reasons exposed above, in this paper, a low-voltage unipolar type dc microgrid is studied. PVA which is less controllable acts as primary power source, its output power is highly dependent on weather conditions (e.g., ambient temperature $T$ and solar radiation $S$ ). For instance, during cloudy periods or at night, PVA would not generate any power. FC which is more controllable is used as backup power. It can operate continuously to supplement as long as the fuel is sufficient. But taking the inherent nature of FC into account, instantaneous power demand will cause fuel starvation, thus affecting its performance and lifetime [11], therefore SC is necessary to provide the transient power demand. In order to supply an uninterrupted, high efficiency, and high quality power to variable dc loads, power control and energy management strategy are proposed, which must have the following functions: 1) optimal energy utilization can be realized, 2) power variation of FC should be limited, 3) the upper/lower limits of state of charge (SoC) for SC must be considered; and 4) system can operate in either grid-connected or islanded mode. Simulation model with considering the characteristics of DGs is developed to verify the system performance under different scenarios.

## 2. System Configuration and Model

### 2.1 System configuration

Figure 1 shows a simple scheme of the studied dc microgrid, which consists of PVA, FC, SC, power electronic interfaces, dc distribution line and dc loads. Different energy/storage sources are integrated through an common dc bus, forming a hybrid distributed generation system (HDGS), then it is connected to utility grid via a three-phase voltage source rectifier (VSR). The dc distribution line is assumed to be lossless and all dc loads are fed by dc bus. Three types of power electronic interfaces are used in this system, namely boost converter, bidirectional dc/dc converter and VSR.

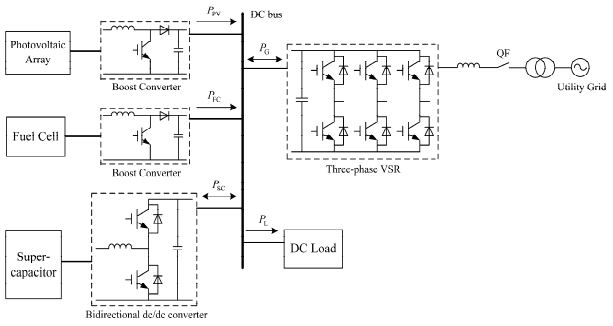


Fig.1. The configuration of the studied dc microgrid

### 2.2 Modeling of PVA

In order to provide the desired output terminal voltage and current, many cells are connected in series and parallel

to form PVA. Figure 2 shows the equivalent circuit of a photovoltaic (PV) cell.

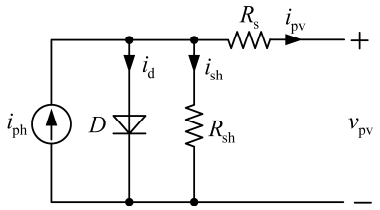


Fig. 2. The equivalent circuit of a PV cell

Equation (1) gives the relation between voltage and current.

$$i_{pv} = i_{ph} - I_o \cdot \left[ \exp\left( \frac{v_{pv} + R_s i_{pv}}{\alpha \cdot V_t} \right) - 1 \right] - \frac{v_{pv} + R_s i_{pv}}{R_{sh}} \quad (1)$$

where $i_{ph}$ and $I_o$ are the PV and saturation currents of the array, respectively, and $V_t = N_s kT / q$ is the thermal voltage. $R_s$ is the equivalent series resistance, $R_{sh}$ is the equivalent parallel resistance. For the details of model development, the reader is referred to [12].

### 2.3 Modeling of FC

Because of the low operating temperature and fast start up, proton exchange membrane (PEM) fuel cell has been found to be especially suitable for residential and commercial applications. The model reported in [12] is used in this paper and the output voltage of a single cell can be defined as the result of the following equations,

$$V_{FC} = E_{Nernst} - V_{act} - V_{ohmic} - V_{con} \quad (2)$$

where $E_{Nernst}$ is the thermodynamic potential representing its reversible voltage, $V_{act}$ is the activation voltage drop, $V_{ohmic}$ is the ohmic voltage drop, and $V_{con}$ is the concentration voltage drop.

## 3. Energy Management Strategy

For the satisfactory operation of the dc microgrid especially during transient and islanding, an overall control strategy for power management among different energy sources is needed. In this paragraph, control objective, operation mode and operating strategy are discussed, sequentially.

### 3.1 Control objective

The control objective that should be met for power management strategy can be summarized as follows.

1) The control scheme of network and storage converters is based on the control loop feedback of the dc voltage, since this is the only common signal for power balancing within the dc microgrid.

2) The dc bus voltage must be well maintained with a limited variation band ( $\pm 5\%$ ) under any condition.

3) The low-cost solar energy is given the first priority in satisfying power demand to minimize economic cost of the overall system, and maximum power point tracking (MPPT) of the PVA must be implemented since it makes the system efficient.

4) The power variation ratio of FC is limited within a preset value to avoid gas starvation and the output power of FC must be kept within an interval $[0, P_{FCRated}]$.

5) The terminal voltage of SC is kept within an interval $[V_{SCMin}, V_{SCMax}]$ to avoid overcharging and deep discharging. Moreover, the current is also required to be within $[-I_{SCRated}, I_{SCRated}]$.

### 3.2 Operation mode

The operation of the system is categorized into four modes: Mode 1 (islanding mode with FC discharging), Mode 2 (islanding mode with SC charging), Mode 3 (grid-connected mode with rectification), and Mode 4 (grid-connected mode with inversion). Four operating modes are described as follows.

Mode 1, in this mode, system operates in islanding mode and dc bus voltage is regulated by SC. Because the solar generation is less than dc load demand, FC is used to provide the gap power while SC supplies the peak power demand. Neglecting the power losses, there is

$$P_{FC} + P_{SC} = P_L - P_{PV} \quad (3)$$

where $P_{FC}$ is the power generated by FC, $P_{SC}$ refers to the power from the SC system, $P_L$ is the load demand, and $P_{PV}$ is the power generated by PVA.

Mode 2, this mode corresponds to island operation and dc bus voltage is also controlled by SC. At this time, the maximum power of PVA is greater than the dc load demand, and SC is charged by surplus power. Therefore, the power balance equation can be written as

$$P_{PV} = P_L + P_{SC} \quad (4)$$

But if the stored energy becomes over the maximum limit, SC must stop working and PVA should switch its control from tracking maximum power to limiting power output to control the dc bus voltage. Another way is to utilize the electrolyzer to yield hydrogen for future use. In this study, the former one is adopted.

Mode 3, this mode refers to ac grid connection operation via the three-phase VSR which allows bidirectional power flow. In this mode, dc bus voltage is controlled by VSR through rectification, which means the solar generation is less than the total loads at the dc side, and the required power from the utility grid is

$$P_G = P_L - P_{PV} \quad (5)$$

where $P_G$ is the power input to the dc microgrid from the VSR.

Mode 4, in this mode, the system operates with connection to ac grid through bidirectional VSR. The dc bus voltage is regulated by VSR through inversion, which means that the generated power is greater than the dc load demand. The excess power is transfered from dc side to ac grid. Therefore, the power balance equation for this situation can be written as

$$P_{PV} = P_L + P_G \quad (6)$$

The working state of the system is shown in Table 1. It can be noticed that PVA achieves its maximum power during mode 1, mode 3 and mode 4. During mode 2, PVA operates at maximum power point (MPP) before SC is fully charged. Otherwise, PVA is operating with constant voltage (CV) control.

### 3.3 Operating strategy

The operating strategy is designed to satisfy load demand under different operating conditions. The necessary measurements are performed and measurement results are conveyed to the microgrid central controller (MGCC) which evaluates the inputs and takes the required actions to provide the overall controls. Fig. 3 shows the flow chart of the MGCC, and the operating strategies used are as follows:

1) Normally, the dc network operates in grid-tied mode. When severe faulty conditions are detected, the dc microgrid is isolated from the ac grid by blocking the switching signals to the switches.

Table 1. The working state of the system under different operation modes

| Mode | Islanding/ Grid-tied | PVA | SC | FC | Exchange power | DC bus control | Load demand |
|---|---|---|---|---|---|---|---|
| 1 | Islanding | MPPT | Discharging | Discharging | $P_G = 0$ | SC Converter | $P_{PV} < P_L$ |
| 2 | Islanding | MPPT or CV control | Charging or not work | Not work | $P_G = 0$ | SC or PVA Converter | $P_{PV} > P_L$ |
| 3 | Grid-tied | MPPT | Not work | Not work | $P_G > 0$ | VSR | $P_{PV} < P_L$ |
| 4 | Grid-tied | MPPT | Not work | Not work | $P_G < 0$ | VSR | $P_{PV} > P_L$ |

2) In grid-tied mode, power is balanced by the utility grid, and the dc voltage is also regulated by VSR. SC and FC do not work to make maximum fuel savings.

3) In islanded mode, SC plays a very important role for voltage stability, and FC is responsible for power balance. SC not only provides the peak electricity demand, but also compensates the tracking mismatches and delays of the FC system which has relatively slow response time.

4) When the stored energy becomes over the maximum limit or under the minimum limit, SC should stop working to avoid full-charged or full-discharged.

5) The control method of PVA is switched from MPPT to CV control if SC is fully charged.

6) When the discharge is limited and FC system up to the maximum limit, specific loads that do not need high-quality power have to be switched out to make the terminal voltage of SC become within the limits.

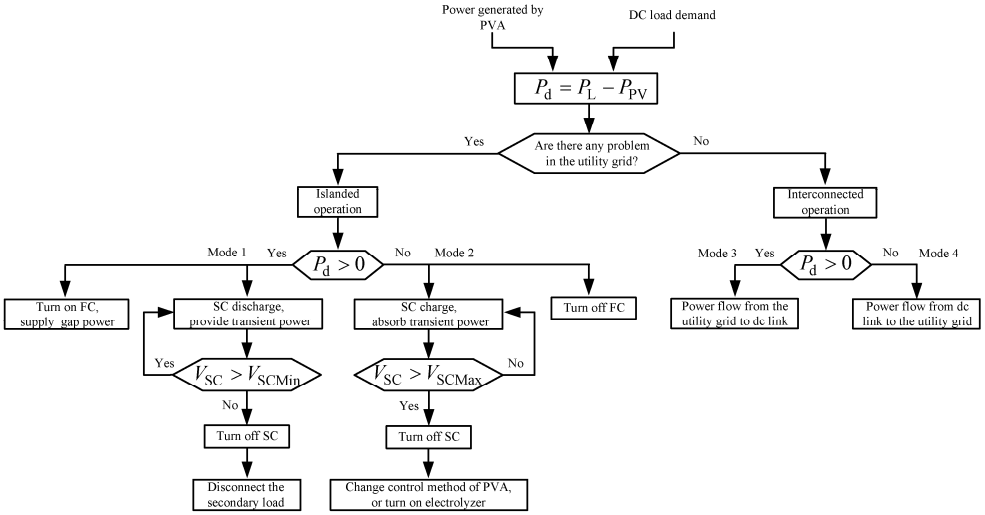


Fig.3. Flow chart of the control algorithm used in MGCC

## 4. Control Scheme for Converters

### 4.1 Islanding operation

For PVA system, either MPPT or CV control is implemented, as shown in Fig. 4. PVA state depends only on the terminal voltage of SC ( $V_{SC}$ ). When $V_{SC}$ exceeds the maximum voltage $V_{SCMax}$ , $K$ becomes 0, and the control mode is switched. Where $D_{PV}$ is the duty cycle of the PVA side boost converter, independent of any other variables. Fractional open circuit voltage method [13] is used in this study to track the maximum power by making the output voltage $V_{PV}$ to reach the voltage at the maximum power point $V_m$. In addition, in order to improve the efficiency of boost converter at low irradiance, PVA does not work until the solar radiation is higher than 100W/m$^2$.

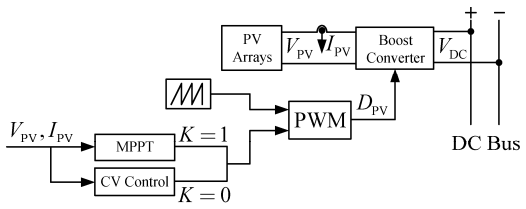


Fig. 4. Schematic diagram of the PVA control system

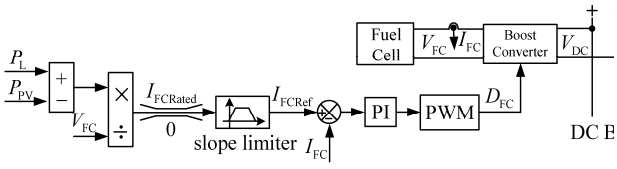


Fig. 5. Block diagram of the control scheme for FC

As previously described, when dc microgrid operates in islanding mode, any power deficit between solar generation and user demand should be supplied by FC stack through proper control of $D_{FC}$ , which is the duty cycle of the FC side boost converter. FC has two working state: off and discharge. When the available power from PVA exceeds the load demand, FC remains off. Once PVA cannot satisfy the demand of dc loads, FC comes online and starts to discharge. Fig. 5 shows the block diagram of the implemented control scheme. $P_L$ is the load demand and compared with the solar generation $P_{PV}$ . Then, the difference is divided by FC voltage $V_{FC}$ to obtain the required current, which must be kept within an interval $[0, I_{FCRated}]$ . Due to the slow response time of FC, current variation versus time limitation is implemented by slope limiter to reduce stress and assure them a sufficient life-

time. Conventional PI controller associated to a pulse width modulation (PWM) generator is selected to directly control the FC current $I_{\mathrm{FC}}$.

SC is connected to dc bus by a bidirectional dc/dc converter, which operates as a boost converter when $D_3$ and $S_4$ are at work with power flow from SC to dc link. On the contrary, it operates as a buck converter when $D_4$ and $S_3$ are working with power flow in the opposite direction. SC has three modes: charge, discharge and off. A sudden increase of dc loads or a sudden drop of solar radiation will cause the power shortage at dc grid, and SC is discharging to provide the transient power. Similarly, when dc system operates in mode 2, SC is charged by excess power. Fig. 6 depicts the control scheme for SC converter. A configuration with outer voltage loop plus inner current loop is proposed to maintain a constant dc voltage. The bidirectional dc/dc converter is driven by use of complementary pulses, generated by a hysteresis comparator which is chosen for SC current control, and a classical PI corrector is used to compensate the output voltage variation. SC current has no time-variation limitation in order to achieve the most effective output voltage regulation. Additionally, the SC limitation function described by equation (7) is used to prevent overcharge and overdischarge, and to limit the current reference $I_{\mathrm{SCRef}}$ to the interval $[I_{\mathrm{SCMin}}, I_{\mathrm{SCMax}}]$ [14].

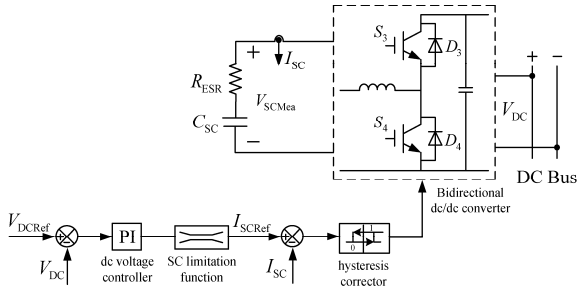


Fig. 6. The control scheme for SC converter

$$\begin{cases} I_{\mathrm{SCMin}} = -I_{\mathrm{SCRated}} \cdot \min\left(1, \dfrac{V_{\mathrm{SCMax}} - V_{\mathrm{SCMea}}}{\Delta v}\right) \\ I_{\mathrm{SCMax}} = I_{\mathrm{SCRated}} \cdot \min\left(1, \dfrac{V_{\mathrm{SCMea}} - V_{\mathrm{SCMin}}}{\Delta v}\right) \end{cases} \tag{7}$$

where $V_{\mathrm{SCMin}}$ and $V_{\mathrm{SCMax}}$ are the lowest and highest acceptable voltage of SC, respectively. $V_{\mathrm{SCMea}}$ is the measured terminal voltage of SC, and $\Delta v$ being regulation parameter.

### 4.2 Interconnected operation

From Table 1, we know that PVA always work at MPP during interconnected operation. Any power surplus or deficit within dc microgrid is automatically balanced by the connected utility grid through three-phase VSR, and dc voltage is also regulated by VSR. The control scheme consisting of an outer voltage regulator with an inner current control loop, reported in [15], is adopted for three-phase VSR control, as shown in Fig. 7.

From Fig.7, it can be seen that the d-axis current reference ( $i_{\mathrm{gd}}^{*}$ ) is calculated from the outer voltage PI regulator whose input is the difference between the desired ($V_{\mathrm{DCRef}}$) and actual dc voltages ($V_{\mathrm{DC}}$). Two inner current PI controllers based on d-q decoupling control are used for real and reactive power control respectively. Where, the $d$ axis current corresponds to the active power whereas the $q$ axis current refers to the reactive power. The inner current control loop is designed to respond faster than the outer voltage control loop so that the two control loops can be designed independently. Additionally, the feed-forward grid voltage compensation is also used to effectively eliminate the grid harmonics disturbance and fast dynamic response.

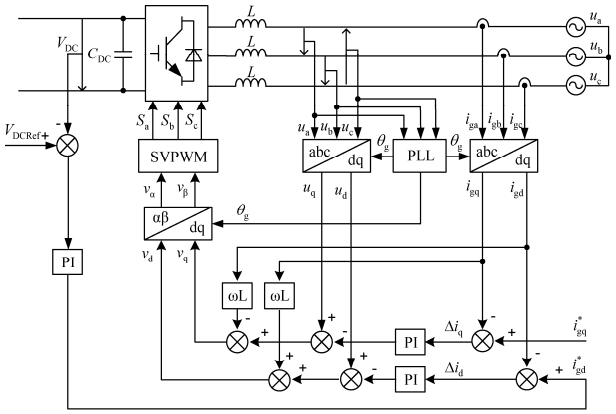


Fig. 7. The control block diagram for the three-phase VSR

### 5. Simulation Result and Analysis

The model including system parameters as shown in Fig. 8 has been simulated by Matlab/Simulink software. Under the assumption that the average load demand is 5kW, the peak load is 30kW, and the maximum fluctuation of load power is 25kW. The PVA size (at MPP) is equal to the expected load power,

$$P_{\mathrm{PVRated}} = \bar{P}_{\mathrm{dem}} / k_{\mathrm{PV}} = 5 / 14.45\% = 34.6\mathrm{kW} \tag{8}$$

where $k_{\mathrm{PV}}$ is the capacity factor of the PVA [16]. To reliably supply dc loads during cloudy periods or at night when dc microgrid operates in stand-alone mode, the rated power of FC must be greater than the peak load (30kW), so in this study the chosen generation capacity of FC is 36kW. Because PEM fuel cell can start up for a few seconds, energy storage does not need a large capacity. The initial voltage of SC is 256V, the minimum and maximum accepted values for SC are 150V and 300V, respectively, and the rated current is 400A. According to [4], dc bus voltage is chosen as 326V. The current ripple and voltage ripple are 10% and 5%, respectively.

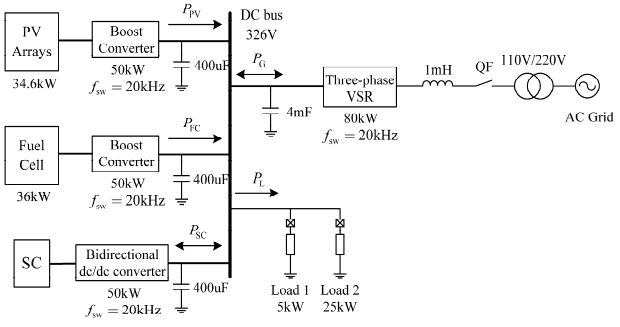


Fig. 8. Schematic diagram of the simulated system

Three kinds of simulation scenarios are carried out to verify the proposed control algorithm. They are as follows: Case 1) dc microgrid operates in stand-alone mode with irradiance and load variations; Case 2) dc system is connected to an external ac grid; and Case 3) the transition process between islanded operation and interconnected operation are also investigated. Simulation results for these scenarios are given and discussed in the following section.

### 5.1 Case 1

To investigate the transient response of dc bus voltage controllers, dc load demand and solar radiation are changed in step, as shown in Fig. 9 and Fig. 10, respectively. The power generated by PVA system is demonstrated in Fig. 11. Table 2 lists the main operation events.

Table 2. Main operation events for case 1

| Events | Operation condition | Time(s) |
|---|---|---|
| 1 | DC loads get down from 30kW to 5kW | 0.15s |
| 2 | Solar radiation increases from 100W/m$^2$ to 400W/m$^2$ | 0.3s |
| 3 | DC loads get up from 5kW to 30kW | 0.35s |
| 4 | Solar radiation reaches 1000W/m$^2$ | 0.45s |
| 5 | Solar radiation drops from 1000W/m$^2$ to 600W/m$^2$ | 0.55s |
| 6 | DC loads decrease from 30kW to 5kW and solar radiation varies from 600W/m$^2$ to 100W/m$^2$ | 0.65s |

The output power of FC and terminal voltage of SC are demonstrated in Fig.12 and 13, respectively.

From t=0s to t=0.15s, the solar generation is unavailable due to low solar radiation, and user demand is 30kW, thus the gap power is 30kW which is provided by both FC and SC. SC supplies the transient power with $V_{SC}$ drop, and the output power of FC linearly increases in a preset slope until $P_{FC}$ is equal to 30kW.

From t=0.15s till t=0.3s, the deficient power is changed from 30kW to 5kW, FC output power gets down from 30kW in a preset slope till the value is equal to 5kW. SC absorbs the transient power with $V_{SC}$ rise.

From t=0.3s till t=0.35s, the solar power is available with generated power 12kW. The solar generation is greater than load demand, and SC is charged by surplus power with $V_{SC}$ rise, at the same time $P_{FC}$ decreases from 5kW to 0kW.

From t=0.35s to t=0.45s, the gap power is 18kW, which is supplied by both FC and SC as mentioned earlier. The subsequent analyses are similar to the previous descriptions, so we will not repeat once again.

Generally speaking, during the time period of t=0s till t=0.3s, t=0.35s till t=0.45s and t=0.55s till t=0.7s the power produced by PVA is less than the dc load demand, FC is used to provide gap power. This means that dc system operates in mode 1. On the contrary, from t=0.3s to t=0.35s and t=0.45s to t=0.55s the generated power is more than user demand, $P_{FC}$ is equal to 0kW and SC is charged by excess power. This situation corresponds to the mode 2.

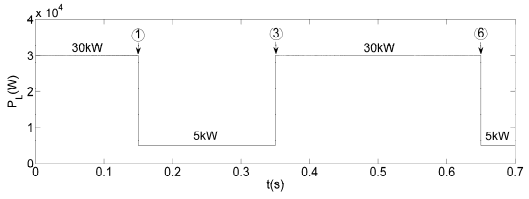


Fig. 9. User demand of the dc microgrid

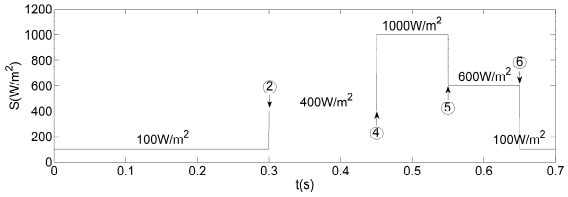


Fig. 10. The variation of solar radiation

Fig. 14 depicts the exchange power between dc microgrid and utility grid during islanded operation. As previously described, when the dc microgrid operates in the stand-alone mode, the VSR is no longer in operation, so the exchange power is 0kW.

The common dc voltage controlled by SC controller is shown in Fig. 15. It can be noticed that the fluctuation of $V_{dc}$ is within the acceptable range ( $\pm 5\%$ ) during variation of irradiance and load demand.

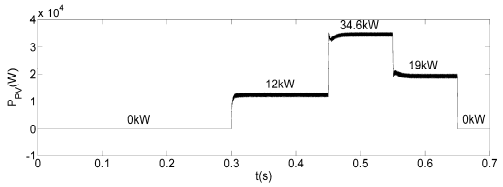


Fig. 11. The output power of PVA

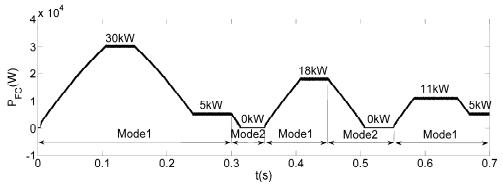


Fig. 12. The output power of FC during islanded operation

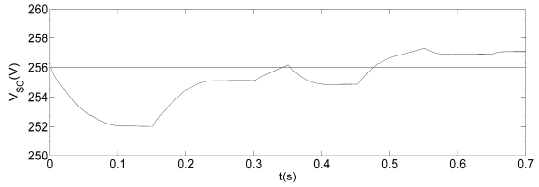


Fig. 13. The terminal voltage of SC during islanded operation

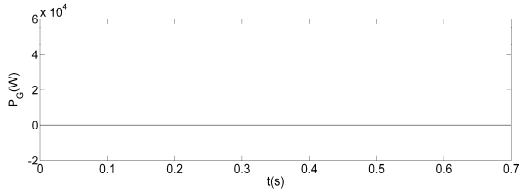


Fig. 14. The exchange power between dc microgrid and utility grid during islanded operation

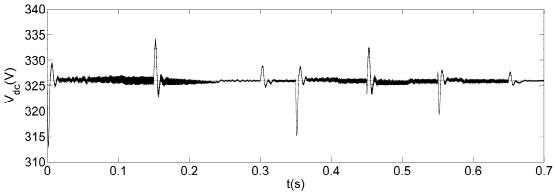


Fig. 15. The dc bus voltage during islanded operation

### 5.2 Case 2

In order to facilitate the study of such scenario, it is assumed that the load demand curve and solar radiation profile used for case 1 are also employed for this case. According to the aforementioned control strategy, it can be concluded that the output power of FC is 0kW, and the terminal voltage of SC is kept constant at initial value, as described in Fig. 16 and Fig. 17, respectively. The reason is that the FC and SC system are not working during interconnected operation.

The exchange power between dc microgrid and utility grid during interconnected operation is recorded as shown in Fig. 18, where positive power region represents the power delivered from the utility grid to dc link (mode 3) and

negative power region represents the power transferred in the opposite direction (mode 4). Since the power factor controlled by VSR is kept at unity, thus the reactive exchange power is equal to 0var all the time. As mentioned earlier, during the time period of t=0s till t=0.15s and t=0.15s till t=0.3s, the gap power is 30kW and 5kW, respectively, which are provided by ac grid. From 0.3s to 0.35s, the excess power (7kW) generated by PVA is delivered from dc link to ac link to keep power balance of the dc microgrid. The rest of this result is not illustrated since the following analysis is exactly the same as the previous principle.

The dc bus voltage during grid-connected operation is shown in Fig. 19. It is obvious that the dc bus voltage remains constant under different operating conditions by using the proposed voltage regulation scheme for network converter.

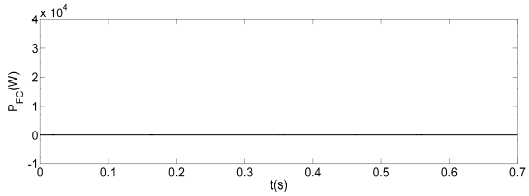


Fig. 16. The output power of FC during grid-tied operation

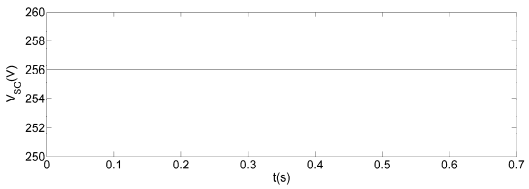


Fig. 17. The terminal voltage of SC during grid-tied operation

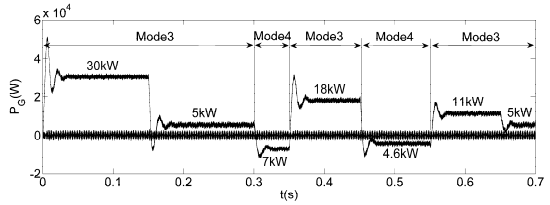


Fig. 18. The exchange power between dc microgrid and utility grid during grid-tied operation

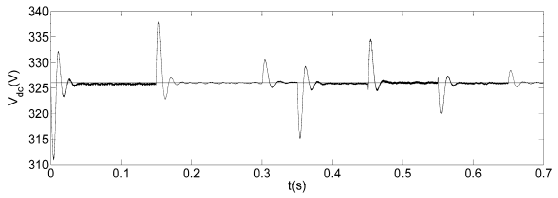


Fig. 19. The dc bus voltage during grid-tied operation

### 5.3 Case 3

In this subsection, we concentrate on investigating whether the dc system can still work stably during the transition process between islanded mode and interconnected mode. Table 3 lists the main operation events for case 3.

Under the condition that the load is equal to 30kW, and solar power generation is 16kW, it can be deduced that FC output power is 14kW during islanded operation, and the exchange power is also equal to 14kW during the period of interconnected operation. The output power of FC and the exchange power between dc microgrid and ac grid are shown in Fig. 20 and 21, respectively.

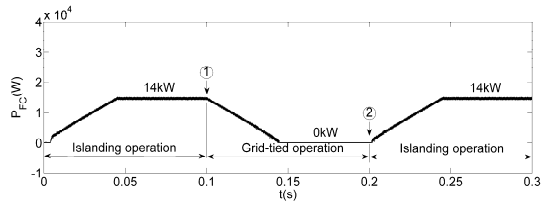


Fig. 20. The output power of FC during transition process

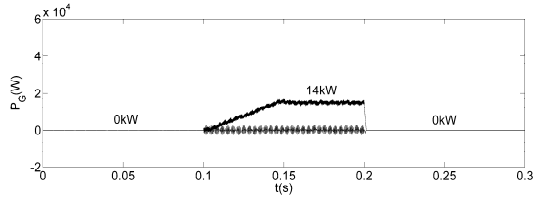


Fig. 21. The exchange power between dc microgrid and utility grid during transition process

Table 3. Main operation events for case 3

| Events | Operation condition | Time(s) |
|---|---|---|
| 1 | DC microgrid is reconnected to ac grid | 0.1s |
| 2 | DC microgrid disconnects from ac grid | 0.2s |

The dc bus voltage variation is demonstrated in Fig. 22. It is obvious that dc bus voltage varies within the limited values during transition process. Also, these results have shown the smooth reconnection and disconnection.

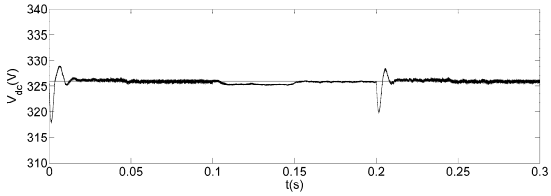


Fig. 22. The dc bus voltage during transition process

## 6. Conclusion

A dc microgrid consisting of PVA, FC, SC, variable loads, and ac grid connection is presented in this paper. The coordinated control schemes are proposed for all the converters to maintain constant dc bus voltage. Three simulation scenarios are designed to verify the proposed control strategy. The results obtained from the research work are as follows:

1) The feasibility of using PVA controller for tracking maximum power from the PVA system is demonstrated.

2) The effectiveness of FC controller for avoiding fuel starvation is verified.

3) The accuracy of storage or network controllers in regulating the dc bus voltage under solar radiation and load demand fluctuations is proved.

4) The dc microgrid can work stably in both grid-connected and islanded mode as well as during switching process.

REFERENCES

[1] Lasseter R.H., Paigi P., Microgrid: a conceptual solution, *IEEE Power Electronics Specialists Conference*, Aachen, Germany, June 2004, 4285-4290

[2] Iyer S.V., Belur M.N., Chandorkar M.C., Analysis and Mitigation of Voltage Offsets in Multi-inverter Microgrids, *IEEE Trans. Energy Conversion*, 26 (2011), No. 1, 354-363

[3] Kakigano H., Nomura M., Ise T., Loss evaluation of DC distribution for residential houses compared with AC system, *The 2010 International Power Electronics Conference* , Sapporo, Japan, June 2010, 480-486

[4] Sannino A., Postiglione G., Bollen M.H.J., Feasibility of a DC network for commercial facilities, *IEEE Trans. Industry Applications*, 39 (2003), No. 5, 1499-1507

[5] Salomonsson D., Sannino A., Low-Voltage DC Distribution System for Commercial Power Systems With Sensitive Electronic Loads, *IEEE Trans. Power Delivery*, 22 (2007) No. 3, 1620-1627
[6] Kakigano H., Miura Y., Ise T., Low-Voltage Bipolar-Type DC Microgrid for Super High Quality Distribution, *IEEE Trans. Power Electronics*, 25 (2010), No. 12, 3066-3075
[7] Salomonsson D., Soder L., Sannino A., Protection of Low-Voltage DC Microgrids, *IEEE Trans. Power Delivery*, 24 (2009) No. 3, 1045-1053
[8] Sun K., Zhang L., Xing Y., Guerrero J.M., A Distributed Control Strategy Based on DC Bus Signaling for Modular Photovoltaic Generation Systems With Battery Energy Storage, *IEEE Trans. Power Electronics*, 26 (2011), No. 10, 3032-3045
[9] Xu L., Chen D., Control and Operation of a DC Microgrid With Variable Generation and Energy Storage, *IEEE Trans. Power Delivery*, 26 (2011), No. 4, 2513-2522
[10] Noroozian R., Abedi M., Gharehpetian G.B., Hosseini S.H., Distributed resources and DC distribution system combination for high power quality, *International Journal of Electrical Power & Energy Systems*, 32 (2010), No. 7, 769-781
[11] Thounthong P., Davat B., Rael S., Sethakul P., Fuel starvation, *IEEE Industry Applications Magazines*, 15 (2009), No. 4, 52-59.
[12] Uzunoglu M.,Onar O. C., Alam M. S., Modeling, control and simulation of a PV/FC/UC based hybrid power generation system for stand-alone applications, *Renewable Energy*, 34 (2009), No.3, 509-520
[13] Esram T., Chapman P. L., Comparison of Photovoltaic Array Maximum Power Point Tracking Techniques, *IEEE Trans. Energy Conversion*, 22 (2007), No. 2, 439-449
[14] Thounthong P., Rael S., Davat B., Control Strategy of Fuel Cell and Supercapacitors Association for a Distributed Generation System, *IEEE Trans. Industrial Electronics*, 54 (2007), No. 6, 3225-3233
[15] Tsai M.T., Tsai W.I., Analysis and design of three-phase AC-to-DC converters with high power factor and near-optimum feedforward, *IEEE Trans. Industrial Electronics*, 46 (1999), No. 3, 535-543.
[16] Wang C.S., Nehrir M.H., Power Management of a Stand-Alone Wind/Photovoltaic/Fuel Cell Energy System, *IEEE Trans. Energy Conversion*, 23 (2008), No. 3, 957-967

***Authors**: Guiting XUE, Department of Electrical Engineering, Shanghai Jiao Tong University, No. 800 of Dongchuan Road, Minhang District, Shanghai, CHINA, xueguiting@163.com*